J Mater Sci: Mater Electron (2010) 21:811–816
DOI 10.1007/s10854-009-9997-x

Phase component and conductivities of Co-doped $BaTiO_3$ thermistors

Jian Wang · Hong Zhang · Yiyu Li · Zhicheng Li

Received: 13 July 2009 / Accepted: 2 October 2009 / Published online: 16 October 2009

Abstract $BaTi_{1-x}Co_xO_{3-\delta}$ $(0.01 \leq x \leq 0.4)$ ceramics were prepared by a wet chemical process polymerized with polyvinyl alcohol. The phases and related electrical properties of the ceramics were investigated. The phase component of the ceramics changes from a tetragonal phase to a hexagonal one with the Co concentration increase. A pure hexagonal phase formed in the ceramic with $x = 0.2$. The measurement of the temperature dependence of resistances revealed that the ceramic resistivities increase with temperature rising at the temperatures (T) lower than half of the related Debye temperature (Θ_D), and the ceramics show a negative temperature coefficient (NTC) effect at $T > \Theta_D/2$. The material constants $B_{50/120}$ of the $BaTi_{1-x}Co_xO_{3-\delta}$ NTC thermistors were calculated to be 3,187, 2,968 and 2,648 K for $x = 0.2$, 0.3 and 0.4, respectively. Narrow-band conduction and non-adiabatic hopping models are proposed for the conduction mechanisms at $T < \Theta_D/2$ and $T > \Theta_D/2$, respectively.

1 Introduction

The thermistors with a characteristic of negative temperature coefficient (NTC) of resistivity are widely used in various industrial and domestic applications. Traditionally, most of the NTC thermistors are based on the solid solutions of transition metal oxides with a spinel structure, such as Mn–Ni–O, Mn–Ni–Cu–O and Mn–Co–Ni–O systems [1–3]. For the interesting electrical property, lots of scientists and engineers have also focused on the doping effect of the spinel type NTC thermistors, e.g., MgO, Al_2O_3 and Cr_2O_3 doped NTC thermistors [4–6], Cu and/or Zn doped $Ni_{0.5}Mn_{2.5}O_4$ or $Mn_{1.17-x}Ni_{0.93}Co_{0.9}Zn_xO_4$ [7, 8], and the doping effect of Fe in $Cu_{0.10}Ni_{0.66}Mn_{2.24}O_4$ thermistors [9]. However, the applications of NTC thermistors based on the spinel oxides are commonly limited to the temperatures below 200 °C for the relaxation of the crystal structure at high temperature [10]. For the different applications, some new type of NTC oxides have been developed, such as Bi_2O_3 doped with TiO_2, Ta_2O_5 and WO_3 [11], $Bi_3Zn_2Sb_3O_{14}$ ceramics [12], $BaTiO_3$ co-doped with $BaBiO_3$ and Y_2O_3 [13], and composite of polyaniline and Mn_3O_4 [14], etc.

$BaTiO_3$-based ceramics have been widely studied and applied as the electronic ceramics such as capacitors for their dielectrical properties and thermistors for the effect of positive temperature coefficient (PTC) of resistivity. Meanwhile, it is reported that a hexagonal structure $BaTiO_3$ (h-$BaTiO_3$) can be stabilized at room temperature by rapid quenching from temperatures higher than 1,460 °C [15], firing in reducing atmospheres [16–18], or doping with some acceptor-type ions (e.g., Mg, Al, Cr, Mn, Cu, Fe, Co, Zn, Ga, Ni and In) on Ti site [19–22]. Most of the previous researches on h-$BaTiO_3$ focused on the phase transformation. However, as our knowledge, there has not been any report on the NTC effect of h-$BaTiO_3$ ceramics so far. During investigating the influence of Co doping on the crystal structure and electrical property of the $BaTi_{1-x}Co_xO_{3-\delta}$ ceramics, the authors found that the $BaTi_{1-x}Co_xO_{3-\delta}$ ceramics can not only transform from a tetragonal

J. Wang · H. Zhang · Y. Li · Z. Li (✉)
School of Materials Science and Engineering,
Central South University, 410083 Changsha, Hunan,
People's Republic of China
e-mail: zhchli@mail.csu.edu.cn

J. Wang · H. Zhang · Y. Li · Z. Li
State Key Laboratory of Powder Metallurgy,
Central South University, 410083 Changsha, Hunan,
People's Republic of China

structure to a hexagonal one when the Co concentration increases, but also, more interesting, display an excellent NTC effect. The investigation results about the phase transformation and temperature dependence of resistivity in the $BaTi_{1-x}Co_xO_{3-\delta}$ ceramics are reported in present paper.

2 Experimental

Appropriate quantities of barium carbonate ($BaCO_3$,), tetra-*n*-butyl titanate (TBT) and cobalt oxide (Co_2O_3) were weighed according to the given formula $BaTi_{1-x}Co_xO_{3-\delta}$ ($x = 0.01, 0.05, 0.1, 0.2, 0.3, 0.4$), respectively. TBT was dissolved in anhydrous alcohol, $BaCO_3$ and Co_2O_3 were dissolved in dilute nitric acid, respectively. And then the above solutions were mixed together. Proper quantity of polyvinyl alcohol was employed as polymeric carrier in the solution mixture [23]. The obtained solution was heated and dried under magnetically stirring to form precursor. The precursors were calcined at 850 °C for 2 h, and then were pressed into pellets in about 15 mm in diameter and 3.5 mm in thickness. The glue pellets were sintered at 1,300 °C for 2 h in air. The sintered pellets were ground to a thickness of about 2 mm and painted with silver paste on both parallel sides of the samples as the electrode.

The temperature dependence of resistance (*R–T*) of the samples was measured by an *R–T* measurement system (ZWX-C, HuaZhong University of Science and Technology, China), and the temperature dependence of resistivity (ρ–*T*) was calculated according to the related sample size. The test temperature ranges from 26 to 300 °C. The phase components of the prepared ceramics were examined by an X-ray diffractometer (D/MAX 2550 PC) with Cu K_α radiation. The microstructures of the $BaTi_{0.8}Co_{0.2}O_{3-\delta}$ ceramics were investigated with a scanning electron microscope (SEM) (JEOL, JSM-6360LV) and a transmission electron microscope (TEM) (FEI Tecnai G^2 F20), respectively.

3 Results and discussion

3.1 Phase analysis

Figure 1 shows the XRD patterns of the as-sintered ceramics with different Co concentrations. For $x = 0.01$, a pure tetragonal phase (marked by '▼') can only be detected in the ceramic. It indicates that the $BaTi_{0.99}Co_{0.01}O_3$ ceramic has the similar phase composition as that of $BaTiO_3$. The lattice parameter was determined to be $a = 0.3996$ nm and $c = 0.4019$ nm. As the Co concentration increases, e.g. $x = 0.05$, some diffraction peaks belonging to a hexagonal phase, $(10\bar{1}3)$, $(20\bar{2}3)$ and $(10\bar{1}7)$, can be detected besides the ones from the tetragonal phase. These indicate that a hexagonal phase formed and the ceramics is composed of the tetragonal and hexagonal phases. The peak intensity from the hexagonal phase increases, while those from the tetragonal phase decreases, with the Co concentration increases. It is found from Fig. 1 that the $x = 0.2$ ceramic has a single phase of a hexagonal polymorph with the space group of $P6_3/mmc$. The lattice parameter can be determined to be $a = 0.5708$ nm and $c = 1.3987$ nm. In the ceramics with $x = 0.3$ and $x = 0.4$, two extra diffraction peaks as marked by '◆' from an impurity can be detected at $2\theta = 28.5°–30°$. The impurities were determined to be Ba_2TiO_4.

Figure 2a is a SEM observation of the as-sintered $BaTi_{0.8}Co_{0.2}O_{3-\delta}$ ceramic. The ceramic has the grain size about 5 μm. Some pores, which should result from the volatilization of cobalt atoms during sintering, can be seen in the ceramic. The analysis of X-ray energy dispersive

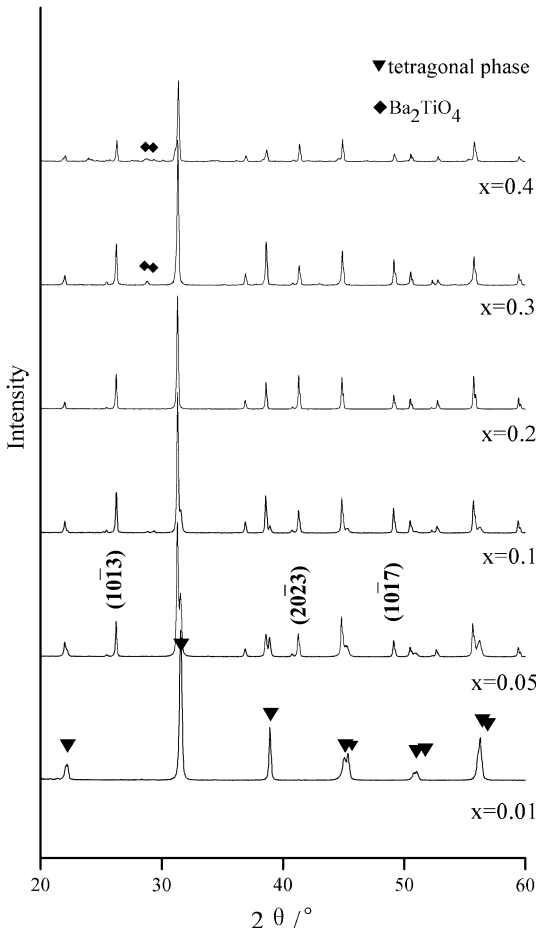

Fig. 1 XRD patterns of the as-sintered $BaTi_{1-x}Co_xO_{3-\delta}$ ceramics ($x = 0.01, 0.05, 0.1, 0.2, 0.3, 0.4$), ▼ indicates the tetragonal phase, ◆ indicates the Ba_2TiO_4 phase, the other peaks belong to the hexagonal phase

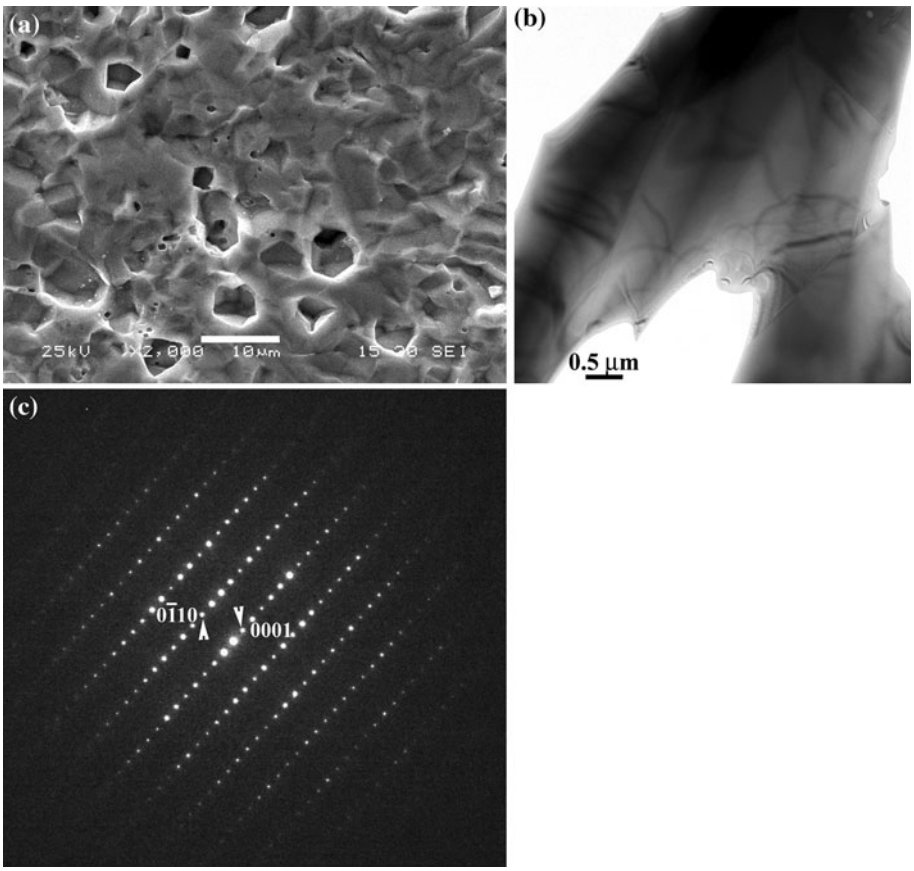

Fig. 2 Microstructure investigation of the $BaTi_{0.8}Co_{0.2}O_{3-\delta}$ ceramics: **a** SEM image, **b** TEM image, and **c** a SAED pattern

(EDX) shown that all the grains have the similar composition with Ba, Ti, Co and O. The EDX is not shown here. During TEM investigation, only hexagonal phase was observed. Figure 2b is a TEM image of the $BaTi_{0.8}Co_{0.2}O_{3-\delta}$ ceramic. A selected-area-electron diffraction (SAED) pattern taken from the center grain, in Fig. 2b, along $[2\bar{1}\bar{1}0]$ direction, is shown in Fig. 2c. Two diffraction points marked by arrows were indexed in Fig. 2c, indicating the hexagonal structure as described in Fig. 1.

It is commonly accepted that the oxygen deficiency plays a key role in stabilizing the h-$BaTiO_3$ at room temperature. Both the Rietveld refinement of neutron diffraction data and study of density functional theory suggested that oxygen nonstoichiometry occurs by removal of O(1) from $Ba(1)O(1)_3$ layers which separate the pairs of occupied face-sharing Ti_2O_9 octahedra (see in Fig. 3) [24, 25]. In undoped case, the oxygen-loss, which is chargedly compensated by partial reduction of Ti^{4+} to Ti^{3+}, plays an important role in the reduction of the Gibbs energy and in the retention of the h-$BaTiO_3$. The hexagonal phase increased proportionally to the amount of Ti^{3+} ions by the reduction of Ti^{4+} ions, and the minimal concentration of Ti^{3+} for stabilizing the hexagonal $BaTiO_3$ at room temperature was 0.3% of the total Ti ions [17]. On the other hand, the transformation temperature from cubic phase to hexagonal one is also related to the concentration of equilibrium oxygen deficiency or Jahn–Teller effect induced by accepter dopants. Co atom has an electronic configuration of $3d^74s^2$ and may lose two or three electrons in compounds. Co^{2+} and Co^{3+} ions are easy to substitute for Ti^{4+} site because of that the radius of either Co^{2+} or Co^{3+} (r_{Co2+}= 79 pm,r_{Co3+}= 68.5 pm) is much less than that of Ba^{2+} (149 pm) and is close to that of Ti^{4+} (74.5 pm) (www.webelements.com). Both Co^{2+} and Co^{3+} ions always substitute for Ti(2) site and have the lowest energy when they are located within the same Ti_2O_9 octahedra [25]. The $BaTi_{1-x}Co_xO_{3-\delta}$ ceramics are expected to lose a slight amount of oxygen by the doping of Co ions in accordance with the following reaction:

$$O_O^{\times} \rightarrow \frac{1}{2}O_2 + V_O^{\bullet\bullet} + 2e' \quad (1)$$

where $O_O^{\times}$ is neutral oxygen, $V_O^{\bullet\bullet}$ is the doubly ionized oxygen vacancy, e' is the electron.

The $BaTi_{1-x}Co_xO_{3-\delta}$ ceramics with a low level of Co concentration (e.g. $x < 0.05$) do not have much enough oxygen vacancies for the full transition from tetragonal phase to hexagonal one, and still contain the tetragonal phase. With the Co concentration increase, the amount of oxygen vacancies increases. More and more octahedrons

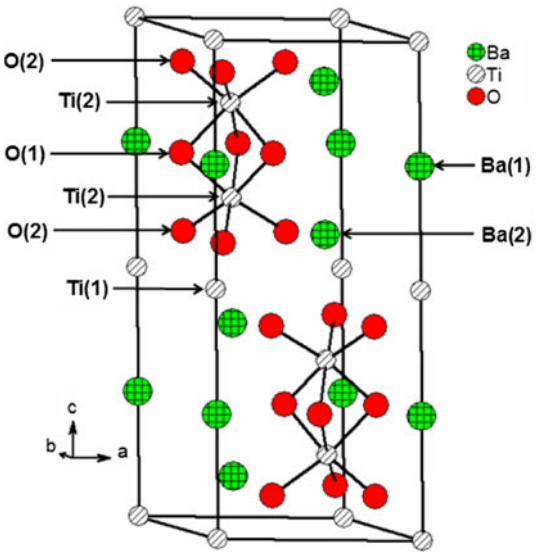

Fig. 3 Illustration of the crystal structure of the h-$BaTiO_3$

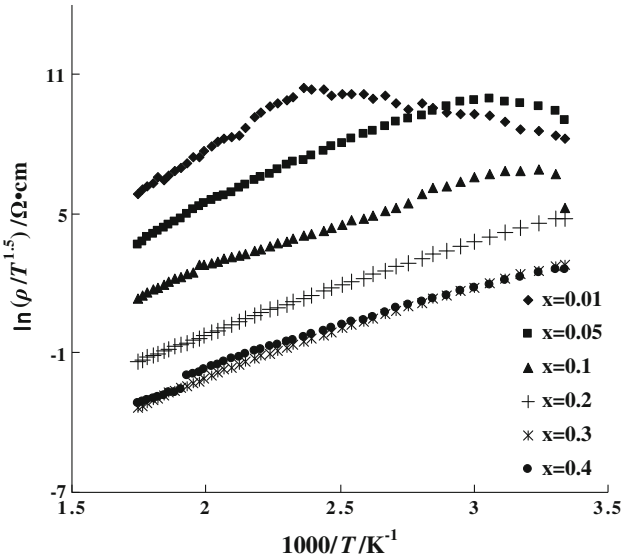

Fig. 4 Temperature dependence of resistivity of the $BaTi_{1-x}Co_xO_{3-\delta}$ ceramics ($x = 0.01$, 0.05, 0.1, 0.2, 0.3, 0.4) by the $\ln(\rho/T^{1.5})$ versus $1000/T$ plots

convert from the corner-sharing structure to the face-sharing one, and the amount of the hexagonal phase increases. As a result, a single hexagonal phase can be obtained when the concentration of Co dopant is high enough, in present experiment, $x \geq 0.2$. On the other hand, because of the volatilization of Co element during the high temperature treatment such as calcining and sintering, the Ba-rich region could form. As a result, the Ba_2TiO_4 phase as showed in Fig. 1 might occur in the ceramics with $x > 0.2$.

3.2 Electrical property

Figure 4 shows the plots of the temperature dependence of resisitivity, by $\ln(\rho/T^{1.5})$ versus $1000/T$, of the $BaTi_{1-x}Co_xO_{3-\delta}$ ceramics with various Co concentrations after sintering at 1,300 °C. Where, ρ is the ceramic resistivity and T is the temperature in Kelvin degree. For the samples $x = 0.01$, 0.05 and 0.1, when the measurement temperature increases, the resistivities increase at the temperature lower than the related transition temperature $\Theta_D/2$, and then decrease at the temperatures higher than the $\Theta_D/2$. The Θ_D is the Debye temperature [26]. It can be seen that Θ_D decreases with cobalt-concentration rising (see in Table 1). Meanwhile, the $\ln(\rho/T^{1.5})$ behaves linear dependence of $1000/T$ at $T > \Theta_D/2$. The nonlinear variation of $\ln(\rho/T^{1.5})$ versus $1000/T$ plots at $\Theta_D/2$ often shows evidence of small polaron hopping conduction [27].

However, in the samples of $x \geq 0.2$, the resistivities monotonously decrease with the temperature increase in all the test temperature range, meaning that these samples show the pure NTC effect. It is assumed that $\Theta_D/2$ in these samples is less than the measurement temperatures, 26 °C. The material constants $B_{50/120}$ of the ceramics showing pure NTC effect in the test temperature range can be expressed by:

$$B = \frac{\ln \rho_2 - \ln \rho_1}{1/T_2 - 1/T_1} \quad (2)$$

where ρ_1 and ρ_2 are the resistivities at temperatures T_1 and T_2, respectively. So the $B_{50/120}$ constants of the samples with $x = 0.2$, 0.3 and 0.4 can be obtained to be 3,187, 2,968 and 2,648 K, respectively.

Charge transport in transition metal oxides usually occurs through the partially filled $3d$ orbitals. The $3d$ overlap is too small to form a metallic band, but it is sufficient for the charge carrier to migrate through the crystal by electron exchange. If the interaction between the lattice vibrations and the carrier is sufficiently strong, the carrier bandwidth can be small enough to form small polaron. At low temperatures, the polaron tunnels through the crystal in a narrow band, the bandwidth and mobility decrease with temperature rising until the mean free path becomes equal to the lattice spacing. The band model then breaks down and the polaron hops between ions, by either thermal activation over the barrier in a classical sense or phonon-assisted tunneling through the barrier. The former is dominant if the motion of the charge carrier and lattice are coupled adiabatically. Here the small polaron theory is proposed to discuss the conductivity mechanism in $BaTi_{1-x}Co_xO_{3-\delta}$ ceramics.

For $x < 0.2$, one can see from Fig. 4 that the resistivities increase with temperature rising at the temperatures $T < \Theta_D/2$. This can be explained by the polaron conduction in a narrow-band [28, 29]. At low temperature, the

Table 1 Calculated parameters from the resistivity–temperature relationship of the $BaTi_{1-x}Co_xO_{3-\delta}$ ceramics at $T > \Theta_D/2$

x	Activation energy E_a (eV)	Debye temperature Θ_D (°C)	Debye frequency ω_D (10^{13} Hz)	Coupling parameter γ	J_{max} (eV)	Δ (eV)
0.01	0.550191	300	7.49484	22.29441	0.043515	0.308389
0.05	0.368172	108	4.98348	22.43692	0.028934	0.205054
0.1	0.275225	72	4.5126	18.52275	0.0262	0.185679
0.2	0.274536	<52	<4.251	<19.61337	<0.024681	<0.174915
0.3	0.25567	<52	<4.251	<18.26561	<0.024681	<0.174915
0.4	0.228105	<52	<4.251	< 16.29627	<0.024681	<0.174915

polaron moves in Bloch-type bands, the width W of which is determined by the product of the electronic overlap integral J and a vibrational-overlap integral. Thus

$$W = 4J\exp(-S) \tag{3}$$

where $s = \gamma(2n+1)$, $n = 1/\exp(\hbar\omega_0/2k_BT)$, γ is the coupling parameter, $\hbar$ is the Planck constant, k_B is the Boltzmann's constant and ω_0 is the optical phonon frequency. Here, ω_0 is replaced by the Debye frequency ω_D which stands for the maximum of vibration frequency. The values of ω_D of the samples can be obtained as following relation and are presented in Table 1:

$$\omega_D = k_B\Theta_D/\hbar. \tag{4}$$

The bandwidth, which is determined by electronic overlap, tends to a limiting value of $J \approx 3\hbar\omega_0$ at low temperatures ($T < \Theta_D/2$), and the electron–phonon (e–p) interaction can be regarded as a perturbation. Then the bandwidth decreases exponentially with temperature rising due to increasing vibrational overlap. As the bandwidth is reduced, the mobility of charge carrier is assumed thermal degenerate thus the resistivity increase. At higher temperature range ($T > \Theta_D/2$), non-diagonal transitions play a dominant role [28, 29], giving rise to a thermally activated hopping mobility. Thus the resistivity decreases exponentially with the rising temperature, which shows the NTC behavior.

The substitution of Co^{3+} at Ti^{4+} site leads to the formation of vacancies in the oxygen sublattice in order to maintain charge neutrality. Electrons release in this process may be captured by Ti^{4+} or Co^{3+}. Since Ti^{4+} has the inert gas (Ar) configuration and has lower Sanderson electronegativity (1.50) than that of Co^{3+} (2.56) [30], the possibility of generation of Ti^{3+} is very small. Therefore, these materials are expected to contain Co^{2+} states. The NTC behavior at $T > \Theta_D/2$ occurs due to the thermal activated hopping of electrons between Co^{3+}/Co^{2+} pairs:

$$Co^{3+} + Co^{2+} \rightarrow Co^{2+} + Co^{3+}. \tag{5}$$

The expression of conduction at $T > \Theta_D/2$ can be given as: for non-adiabatic hopping [31]

$$\begin{aligned}\rho &= \frac{k_BT\hbar}{ne^2a^2J^2}\left(\frac{E_ak_BT}{\pi}\right)^{1/2}\exp(E_a/k_BT) \\ &= \rho_0\exp(E_a/k_BT)\end{aligned} \tag{6}$$

and for adiabatic hopping

$$\begin{aligned}\rho &= \frac{2\pi k_BT\hbar}{ne^2a^2\omega_0}\exp(E_b/k_BT) \\ &= \rho_1\exp(E_b/k_BT)\end{aligned} \tag{7}$$

where E_a and E_b is the activation energy, ρ_0 and ρ_1 is the pre-exponential factor, $\hbar$ is the Planck constant, k_B is the Boltzmann's constant, n is the density of charge carrier, a is the jump distance.

From Eqs. 6 and 7, the resistivity increases exponentially with temperature rising in a wide temperature range. The pre-exponential factor that is proportional to either T (for adiabatic hopping) or $T^{1.5}$ (for non-adiabatic hopping) only acts a key role when k_BT is approximate to E_a or E_b. The activation energy E_a (or E_b) can be expressed by [32]:

$$\begin{aligned}E_a &= W_d \quad \text{for} \quad T < \Theta_D/4 \\ E_a &= W_h + W_{d/2} \quad \text{for} \quad T > \Theta_D/2\end{aligned} \tag{8}$$

where W_h is the hopping energy, W_d is the disorder energy rising due to the energy difference of the neighboring sites and is significant at very low temperature ($T < \Theta_D/4$). At high temperature ($T > \Theta_D/2$), W_d is small and the activation energy E_a (or E_b) is approximate to W_h, that is $E_a \approx W_h$. As shown in Table 1, E_a decreases with cobalt-concentration rising. This can be explained by considering that the increasing of cobalt concentration causes stronger electron–electron (e–e) interaction determining the bandwidth between Co ions, and causes the less e–p interaction corresponding to hopping process. As a result, the energy required to liberate a free charge carrier is reduced. Thus the activation energy E_a decreases with cobalt-concentration rising

It is suggested that a value of $\gamma > 4$ usually indicates strong e–p interaction, where γ is the coupling parameter and can be estimated from the relation [27]:

$$\gamma = 2W_h/\hbar\omega_0 \tag{9}$$

The large values of γ as presented in Table 1 indicate that the e–p interaction is dominant in those ceramics and is large enough to form polarons.

Emin and Holstein give the condition for non-adiabatic by [28]:

$$J < \left(\frac{k_B T W_h}{\pi}\right)^{1/4} \left(\frac{\hbar\omega_0}{\pi}\right)^{1/2} \tag{10}$$

In order to give the overlap integral J, Holstein uses the relation:

$$J_{max} = 0.67\hbar\omega_0 (T/\Theta_D)^{1/4} \tag{11}$$

and $J < W_h/3$ is given for small polaron model [33]. The values of J_{max} is presented in Table 1 when T/Θ_D is selected a representative value of 3.

According to the equations from 8 to 11, one can get

$$E_a > \Delta \tag{12}$$

as a condition for non-adiabatic ($E_a \approx W_h$), $\Delta = 5.384 \times 10^{-4}\Theta_D$. As shown in Table 1, all the samples accomplish the condition $E_a > \Delta$ and $J_{max} < E_a/3$. So it can be concluded that the conduction mechanism in those samples follows the non-adiabatic small polaron hopping model for $T > \Theta_D/2$ and the narrow-band conduction model for $T < \Theta_D/2$. The ceramics showed excellent NTC effect at $T > \Theta_D/2$.

4 Conclusions

The phase transforms from a tetragonal one to a hexagonal one in the $BaTi_{1-x}Co_xO_{3-\delta}$ ceramics with the Co dopant concentration rising, and a pure hexagonal phase formed when $x = 0.2$. With the Co concentration higher than $x = 0.2$, a small amount of the Ba_2TiO_4 impurity formed besides the hexagonal phase in the $BaTi_{1-x}Co_xO_{3-\delta}$ ceramics. The resistivity-temperature characteristic of the $BaTi_{1-x}Co_xO_{3-\delta}$ ceramics depends on the related Debye temperatures (Θ_D). The resistivity increases with temperature rising at the temperature lower than $\Theta_D/2$, and decreases with temperature rising at the temperature higher than $\Theta_D/2$. The pure NTC effect exists in the ceramics of $x \geq 0.2$ at the temperatures from 26 to 300 °C, and the material constants $B_{50/120}$ are 3,187, 2,968 and 2,648 for $x = 0.2$, 0.3 and 0.4, respectively. The narrow-band conduction and non-adiabatic hopping conduction are proposed for the conduction mechanisms at the temperature ranges $T < \Theta_D/2$ and $T > \Theta_D/2$, respectively.

Acknowledgement The authors acknowledge the support of the National Nature Science Foundation of China (No. 50872155).

References

1. G.D.C. Csete de Györgyfalva, I.M. Reaney, J. Eur. Ceram. Soc. **21**, 2145–2148 (2001)
2. J.F. Gao, D.L. Fang, Z.B. Wang, P.H. Yang, C.S. Chen, Sens. Actuators A Phys. **135**, 472–475 (2007)
3. W.M. Wang, X.C. Liu, F. Gao, C.S. Tian, Ceram. Int. **33**, 459–462 (2007)
4. K. Park, S.J. Kim, J.-G. Kim, S. Nahm, J. Eur. Ceram. Soc. **21**, 2009–2016 (2007)
5. K. Park, I.H. Han, Mater. Sci. Eng. B **119**, 55–60 (2005)
6. K. Park, J.K. Lee, J.-G. Kim, S. Nahm, J. Alloy. Compd. **437**, 211–214 (2007)
7. C.H. Zhao, B.Y. Wang, P.H. Yang, L. Winnubst, C.S. Chen, J. Eur. Ceram. Soc. **28**, 35–40 (2008)
8. K. Park, J.K. Lee, S.-J. Kim, W.-S. Seo, J. Alloy. Compd. **467**, 310–316 (2009)
9. D.L. Fang, C.S. Chen, A.J.A. Winnubst, J. Alloy. Compd. **454**, 286–291 (2008)
10. A. Feltz, W. Polzl, J. Eur. Ceram. Soc. **20**, 2353–2366 (2000)
11. A. Basu, A.W. Brinkman, T. Hashemi, Int. J. Inorg. Mater. **3**, 1219–1221 (2001)
12. M.A.L. Nobre, S. Lanfredi, Appl. Phys. Lett. **82**, 2284–2286 (2003)
13. Y. Luo, X.Y. Liu, G.H. Chen, J. Alloy. Compd. **429**, 335–337 (2007)
14. K. Majid, S. Awasthi, M.L. Singla, Sens. Actuators A Phys. **135**, 113–118 (2007)
15. F.D. Morrison, D.C. Sinclair, J.M. Skakle, A.R. West, J. Am. Ceram. Soc. **81**, 1957–1960 (1999)
16. R.M. Glaister, H.F. Kay, Proc. Phys. Soc. **76**, 763–771 (1960)
17. M. Wakamatsu, N. Takeuchi, G.C. Lai, I. Shingo, Yogyo Kyokaishi **95**, 1181–1185 (1987)
18. H. Arend, L. Kihlborg, J. Am. Ceram. Soc. **52**, 63–65 (1969)
19. G.M. Keith, M.J. Rampling, K. Sarma, N.M. Alford, D.C. Sinclair, J. Eur. Ceram. Soc. **24**, 1721–1724 (2004)
20. H.T. Langhammer, T. Muller, R. Bottcher, V. Mueller, H.-P. Abicht, J. Eur. Ceram. Soc. **24**, 1489–1492 (2004)
21. I.E. Grey, C. Li, L.M.D. Cranswick, R.S. Roth, T.A. Vanderah, J. Solid State Chem. **135**, 312–321 (1998)
22. A. Jana, T.K. Kundu, Mater. Lett. **61**, 1544–1548 (2007)
23. Z.C. Li, H. Zhang, B. Bergman, X.D. Zou, J. Eur. Ceram. Soc. **26**, 2357–2364 (2006)
24. A. Feteira, G.M. Keith, M.J. Rampling, C.A. Kirk et al., Cryst. Eng. **5**, 439–448 (2002)
25. T.A. Colson, M.J.S. Spencer, I. Yarovsky, Comput. Mater. Sci. **34**, 157–165 (2005)
26. I.G. Austin, N.F. Mott, Adv. Phys. **18**, 41–102 (1969)
27. A. Banerjee, S. Pal, E. Rozenberg, B.K. Chaudhuri, J. Phys. Condens. Matter. **13**, 9489–9504 (2001)
28. D. Emin, T. Holstein, Ann. Phys. **53**, 439–520 (1969)
29. I.G. Austein, A.J. Springthorpe, B.A. Smith, C.E. Turner, Proc. Phys. Soc. **90**, 157–174 (1967)
30. R.T. Sanderson, Inorg. Chem. **25**, 3518–3522 (1986)
31. M.H. Brodsky, *Amorphous semiconductors* (Springer, Berlin, NY, 1979)
32. N.F. Mott, E.A. Davis, *Electronic processes in non-crystalline materials*, 2nd edn. (Clarendon, Oxford, 1979)
33. T. Holstein, Ann. Phys. **8**, 343–391 (1959)